A Highly Active Cobalt Catalyst for the General and Selective Hydrogenation of Aromatic Heterocycles

Christof Bauer,[a] Felix Müller,[b] Sercan Keskin,[c] Mirijam Zobel,[b] and Rhett Kempe*[a]

Abstract: Nanostructured earth abundant metal catalysts that mediate important chemical reactions with high efficiency and selectivity are of great interest. This study introduces a synthesis protocol for nanostructured earth abundant metal catalysts. Three components, an inexpensive metal precursor, an easy to synthesize N/C precursor, and a porous support material undergo pyrolysis to give the catalyst material in a simple, single synthesis step. By applying this catalyst synthesis, a highly active cobalt catalyst for the general and selective hydrogenation of aromatic heterocycles could be generated. The reaction is important with regard to organic synthesis and hydrogen storage. The mild reaction conditions observed for quinolines permit the selective hydrogenation of numerous classes of N-, O- and S-heterocyclic compounds such as: quinoxalines, pyridines, pyrroles, indoles, isoquinoline, aciridine amine, phenanthroline, benzofuranes, and benzothiophenes.

Introduction

The reduction of arenes to saturated cyclic compounds is of considerable interest for the production of bulk and fine chemicals as well as the synthesis of pharmaceuticals and agrochemicals.[1] Hydrogenation is an especially attractive reduction protocol since hydrogen is inexpensive and abundantly available and can be produced sustainably.[2] Furthermore, arene hydrogenation is an elegant way to store hydrogen chemically. Here, nanostructured and reusable catalysts are especially interesting.[3] With regard to the selective hydrogenation of N-heterocycles, nanostructured 3d-metal catalysts[4] and especially cobalt catalysts[5,6–9] have been developed. Unfortunately, the applicability or scope of nanostructured 3d-metal catalysts for the general and selective hydrogenation of N-, O-, and S-heterocyclics is rather limited (see below, section substrate scope). The key here might be novel synthesis

protocols for nanostructured 3d-metal catalysts to permit their operation under mild reaction conditions. We introduce a synthesis protocol for nanostructured earth abundant metal catalysts recently.[10] Unfortunately, the flexibility with regards to the ratio of the metal species and the N-doped carbon for embedding the metal species (metal-N/C ratio) can only be altered slightly by employing different (salen) ligands. As a consequence, we have been searching for a catalyst synthesis protocol having a high flexibility with regard of the ratio of N-doped carbon to 3d-metal species. Three components, an inexpensive metal precursor, a N/C precursor, and a porous support material undergo pyrolysis to give the catalyst material in a simple single synthesis step. The catalyst synthesis is highly flexible about the earth abundant metal that is used. The metal and the N/C precursors permit an optimization of the metal-N/C ratio to boost catalyst performance. Small and reactive metal nanoparticles embedded in a microporous N-doped carbon matrix are formed during pyrolysis. By applying our catalyst synthesis, a highly active cobalt catalyst for the selective hydrogenation of aromatic N-, O-, and S-heterocycles could be identified.

Results and Discussion

Our catalyst synthesis procedure, with spatially separated nitrogen/carbon and metal precursors and a (mesoporous) support material, is shown in Figure 1a. First, the nitrogen/carbon precursor meso-octamethylcalix[4]pyrrole was synthesized according to an adapted literature procedure (Supporting Information 2.1).[11] For the catalyst synthesis, silica was impregnated with meso-octamethylcalix[4]pyrrole and the metal precursor cobalt acetate tetrahydrate with a ratio of 4:1 in methanol. After removal of the solvent at 70 °C, the sample was pyrolyzed under a nitrogen atmosphere at 800 °C (Supporting Information 2.2). Thermogravimetric analysis (TGA) shows the

[a] C. Bauer, Prof. Dr. R. Kempe
Inorganic Chemistry II – Catalyst Design
Sustainable Chemistry Centre
University of Bayreuth
95440 Bayreuth (Germany)
E-mail: kempe@uni-bayreuth.de
Homepage: www.sustainable-chemistry-centre.uni-bayreuth.de

[b] F. Müller, Prof. Dr. M. Zobel
Institute of Crystallography
RWTH Aachen University
52066 Aachen (Germany)

[c] Dr. S. Keskin
INM - Leibniz Institute for New Materials
Campus D2 2
66123 Saarbrücken (Germany)
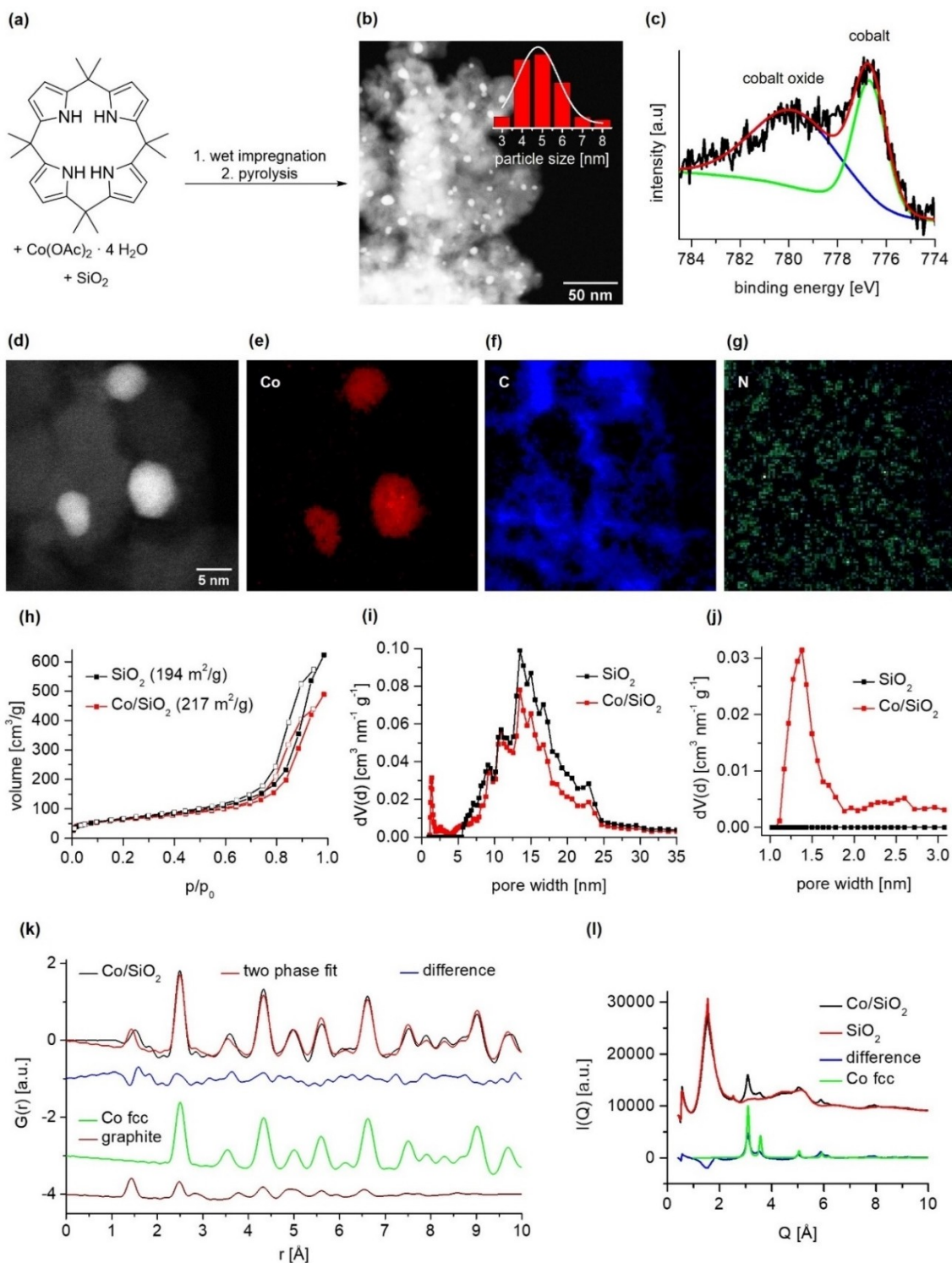
Figure 1. Synthesis and characterization of the Co/SiO₂ catalyst. (a) Synthesis of the cobalt catalyst starting with wet impregnation of meso-ocatmethylcalix[4]pyrrole and Co(OAc)₂·4 H₂O with SiO₂ and subsequent pyrolysis. (b) HAADF-STEM analysis suggests the presence of homogeneously distributed Co nanoparticles with an average particle size of 4.8 nm. (c) XPS analysis of the surface area of the Co 2p$_{3/2}$ area with an asymmetric fit shows Co metal (61%) and cobalt oxide (39%). (d)–(g) HAADF-STEM images of Co/SiO₂ (d), representative EELS element maps of cobalt (e), carbon (f) and nitrogen (g). (h) Surface characterization and (i) pore size distribution of the catalyst via N₂ physisorption measurements (calculation model: N₂ at −196.15 °C: slit/cylindric pore, NLDFT equilibrium model). The specific surface area showed a slight increase from 194 m²/g of the support material to 217 m²/g of the catalyst. (j) Detailed pore size analysis shows the generation of micropores. (k) The PDF of Co/SiO₂ was fitted with a Co fcc phase of 3.1 nm particle diameter and a graphitic domain, both contributions shown in offset. (l) PXRD data of the catalyst Co/SiO₂ and the support material SiO₂, together with their difference (catalyst-support), which is supposed to be the active catalyst phase. The peaks of the active phase can be assigned to a cobalt fcc phase.

Chemistry–A European Journal

Research Article
doi.org/10.1002/chem.202300561

Chemistry Europe
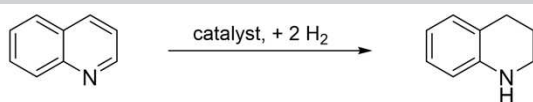European Chemical
Societies Publishing

volatility of the N/C precursor and the decomposition of cobalt acetate under catalyst synthesis conditions (Supporting Information 3.2). Inductively coupled plasma optical emission spectrometry (ICP-OES) analysis of the catalyst revealed a cobalt content of 1.81 wt.% (Supporting Information 3.1). The specific surface area could be determined by nitrogen physisorption measurements (Figure 1h) and showed an increase in surface area from 194 m^2/g for the support material to 217 m^2/g for the catalyst. The pore size distribution of the catalyst material (Figure 1i–j) indicates the generation of additional microporosity compared to the pure silica support material, which is mesoporous. The meso-octamethylcalix[4]pyrrole precursor seems to form a microporous N-doped carbon layer, which embeds the cobalt nanoparticles. The applied 800 °C pyrolysis temperature seem to be optimal for this process. A homogeneous distribution of the cobalt nanoparticles over the support material (Figure 1b) and an average particle size of 4.8 nm could be determined via high-angle annular dark field scanning transmission electron microscopy (HAADF-STEM). In addition, X-ray photoelectron spectroscopy (XPS) showed the presence of metallic cobalt and cobalt oxide on the surface of the catalyst material (Figure 1c). Detailed analysis of the nitrogen area suggests different binding modes of nitrogen within the catalyst (Supporting Information 3.3). Scanning electron microscopy (SEM) in combination with energy dispersive X-ray spectroscopy (EDX) confirmed the homogeneous distribution of the cobalt nanoparticles over silica, as well as nitrogen and carbon (Supporting Information 3.4). The presence of cobalt nanoparticles embedded in a N-doped C matrix on the SiO_2 support was again confirmed using HAADF-STEM in combination with EDX element maps (Supporting Information 3.5). To obtain an insight into the direct environment of the nanoparticles, high resolution HAADF-STEM (Figure d) with electron energy loss spectroscopy (EELS) was performed (Figure e–g). It shows the interface of the support matrix and the cobalt nanoparticles. The carbon component (C, blue) is connected to the cobalt nanoparticles (Co, red) and a signal of nitrogen (N, green) is present in the vicinity of the cobalt nanoparticles as well as in the matrix. Pair distribution function (PDF) studies and corresponding fits (Figure 1k) reveal the active species of the catalyst. Crystalline Co face-centered cubic lattice (fcc) nanoparticles with a spherical shape function indicate a maximum particle size of 3.1 nm (Table S1). The first peak occurring below 1.5 Å is not consistent with pure Co fcc, which has a nearest neighbor distance around 2.51 Å.[12] However, this peak matches very well with a C–C or a C–N bond distance of N-doped graphite, which was formed via pyrolysis.[13] Figure 1l shows the PXRD data of the SiO_2 support and the Co/SiO_2 catalyst. By subtracting the scattering contribution of the pure support material from the catalyst signal, the cobalt loading can be determined. The active sites can be assigned to a Co fcc phase with slightly shifted Q values (Supporting Information 3.6).

To determine suitable reaction conditions for the hydrogenation of aromatic heterocyclic compounds, the hydrogenation of quinoline to 1,2,3,4-tetrahydroquinoline was chosen as a benchmark reaction. The solvent screening revealed that ethanol is the most suitable solvent for the model reaction (Table S2–3). Next the reaction temperature (Table S4) and the hydrogen pressure were screened (Table S5). The optimized parameters of 3 mL ethanol, 2.0 MPa H_2 and 70 °C were determined. The pyrolysis temperature was then varied, and different commercially available support materials and cobalt precursors were tested (Table 1). Lowering the pyrolysis temperature to 700 °C leads to a yield in the trace range, at 600 °C no conversion takes place. With the application of a higher temperature (900 °C) only traces of 1,2,3,4-tetrahydroquinoline were found, indicating the superiority of the catalyst, that was pyrolyzed at 800 °C. Pure SiO_2 support showed no conversion of quinoline. The use of activated carbon as a catalyst support material showed some activity in the selective hydrogenation of quinoline, while cobalt catalysts based on other supports, such as γ-Al_2O_3, TiO_2 and CeO_2 are not suitable for this reaction under the given conditions (Table 1). Further, the use of cobalt acetate is important to the activity of the catalyst. The metal precursors cobalt acetylacetonate, cobalt stearate and cobalt chloride show little to no activity. The only metal precursor with some activity of the final catalyst was cobalt nitrate. We continued our investigation by varying metal loadings of the catalyst. The experiments revealed that the catalyst with theoretically 4.0 wt.% (measured 1.81 wt.%) cobalt showed the best activity (Table S6). Moreover, we examined the effect of the catalyst loading upon catalysis. We observed that the best results were obtained at 5.0 mol% catalyst loading (Table S7). Further, the high activity of our catalyst is based on a specific ratio of the N/C precursor to the cobalt precursor. We assume that a certain amount of microporous N-doped carbon or a certain thickness of the embedding N-doped carbon layer is optimal for educt access and catalyst stability. A layer too thick might prevent educt access and a layer too thin might lead to cobalt leaching since the metal nanoparticles can be more easily removed from the support. Maximum activity in our benchmark reaction is observed if a ratio of metal to C/N precursor of 1:4 is used (M/N ratio). More N-doping leads to a decrease of product yield into a certain plateau at around 60% yield (Table 1). Time conversion studies (Supporting Information 4.2) show that the conversion of quinoline to 1,2,3,4-tetrahydroquinoline is achieved after 17 h under the applied optimal reaction conditions. To ensure completion, a reaction time of 20 h was chosen. In summary, the reaction can be carried out smoothly and selectively with 5 mol% Co, 2.0 MPa H_2, 70 °C and 20 h reaction time. Very mild conditions for the benchmark reaction using nanostructured cobalt catalysts have been disclosed by Beller[5,6] and Zhao[7] and co-workers. Reaction conditions for the work of the Beller group were: 4 mol% Co, 2.0 MPa H_2, 100 °C and 48 h[5] and 9 mol% Co, 1.0 MPa H_2, 70 °C and 24 h.[6] The Co catalyst developed by the Zhao group operates under the following optimal reaction conditions: 2.0 MPa H_2, 100 °C, 3–6 h.[7]

With the optimized reaction conditions in hand, we became interested in the substrate scope of our catalyst system. As shown in Scheme 1, a series of substituted and functionalized quinolines underwent selective hydrogenation to produce aliphatic cyclic derivatives in excellent yields under very mild
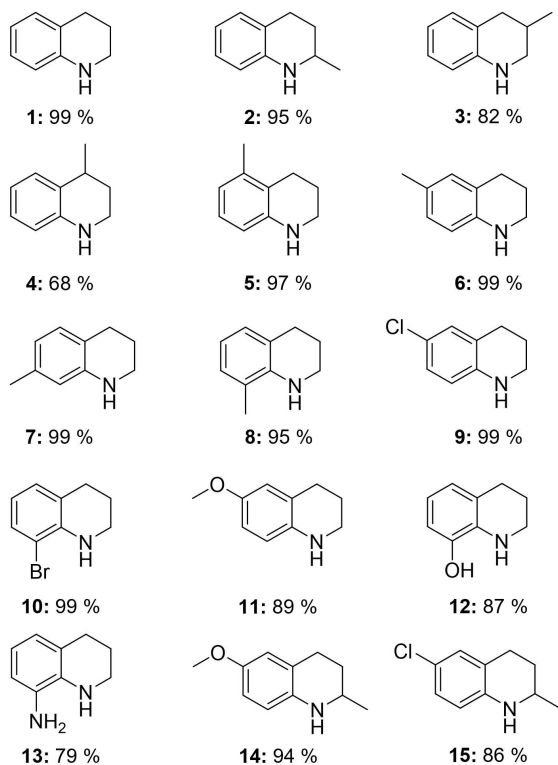
Chemistry–A European Journal

Research Article
doi.org/10.1002/chem.202300561

Chemistry Europe
European Chemical
Societies Publishing

Table 1. Cobalt catalyst comparison.[a]

quinoline $\xrightarrow{\text{catalyst, + 2 H}_2}$ 1,2,3,4-tetrahydroquinoline

Entry	M/N ratio	Metal source	Support material	Pyrolysis temperature [°C]	Yield [%]
1[b]	1:0	$Co(OAc)_2 \cdot 4 H_2O$	SiO_2	800	0
2[b]	1:1	$Co(OAc)_2 \cdot 4 H_2O$	SiO_2	800	traces
3[b]	1:2	$Co(OAc)_2 \cdot 4 H_2O$	SiO_2	800	11
4[b]	1:3	$Co(OAc)_2 \cdot 4 H_2O$	SiO_2	800	16
5[b]	**1:4**	**$Co(OAc)_2 \cdot 4 H_2O$**	**SiO_2**	**800**	**88**
6[b]	1:5	$Co(OAc)_2 \cdot 4 H_2O$	SiO_2	800	62
7[b]	1:10	$Co(OAc)_2 \cdot 4 H_2O$	SiO_2	800	60
8	**1:4**	**$Co(OAc)_2 \cdot 4 H_2O$**	**SiO_2**	**800**	**>99**
9[b]	1:4	$Co(OAc)_2 \cdot 4 H_2O$	SiO_2	600	0
10[b]	1:4	$Co(OAc)_2 \cdot 4 H_2O$	SiO_2	700	traces
11[b]	1:4	$Co(OAc)_2 \cdot 4 H_2O$	SiO_2	800	13
12[b]	1:4	$Co(OAc)_2 \cdot 4 H_2O$	SiO_2	900	traces
13	1:4	$Co(OAc)_2 \cdot 4 H_2O$	activated carbon	800	25
14	1:4	$Co(OAc)_2 \cdot 4 H_2O$	$\gamma\text{-}Al_2O_3$	800	0
15	1:4	$Co(OAc)_2 \cdot 4 H_2O$	TiO_2	800	0
16	1:4	$Co(OAc)_2 \cdot 4 H_2O$	CeO_2	800	0
17	1:4	$Co(acac)_2$	SiO_2	800	0
18	1:4	$Co(NO_3)_2 \cdot 6 H_2O$	SiO_2	800	48
19	1:4	Co(II)stearate	SiO_2	800	9
20	1:4	$CoCl_2 \cdot 6 H_2O$	SiO_2	800	0
21	1:4	–	SiO_2	800	0

[a] Reaction conditions: 5.0 mol% Co (1.81 wt.% Co, 0.01 mmol Co, 0.59 mg Co), 0.2 mmol quinoline, 3 mL ethanol, 70 °C, 2.0 MPa H_2, 20 h. Yields were determined by GC using *n*-dodecane as an internal standard. [b] Same as [a] but 60 °C.
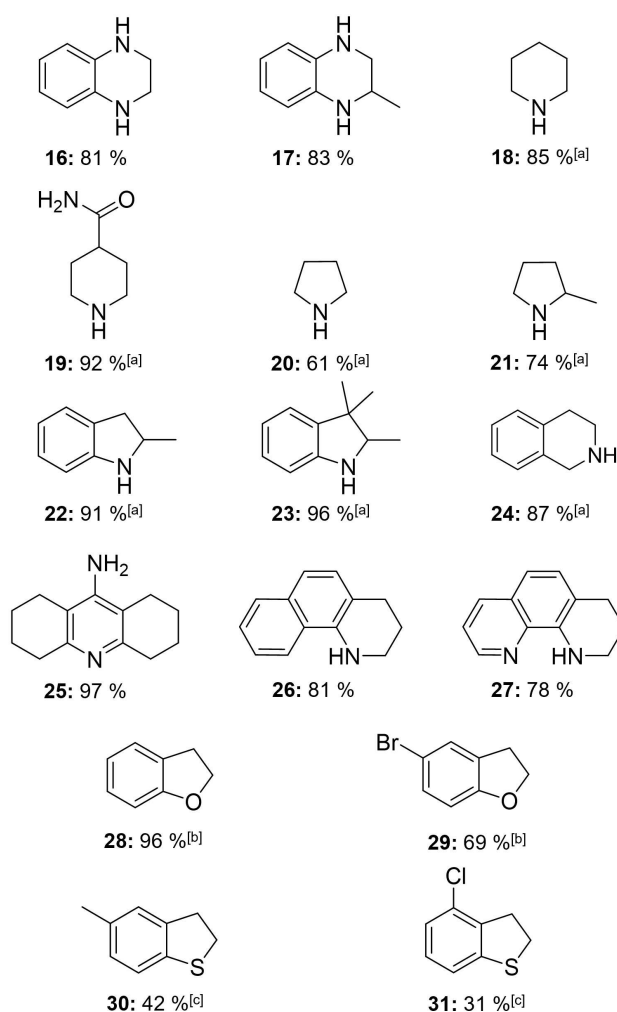
conditions. First, we applied our catalyst for the hydrogenation of pure quinoline and achieved an excellent yield. Subsequent investigations involved fifteen quinoline derivatives, which were hydrogenated also under relatively mild conditions. This led to the formation of 1,2,3,4-tetrahydroquinolines with up to 99% isolated yields (Scheme 1, products **1**, **6**, **7**, **9** and **10**) indicating that the catalytic process is able to proceed with considerable variation in the nature and the position of the substituents. In particular, both electron-donating methyl substituents (Scheme 1, products **2–8**) and electron-withdrawing halogen substituents (Scheme 1, products **9** and **10**) yield the desired product in high yield. Furthermore, the catalyst succeeds when methoxy, hydroxy and amine groups (Scheme 1, products **11–13**) are present. Finally, the catalyst is also able to tolerate two functional groups (Scheme 1, product **14** and **15**) producing the intended 1,2,3,4-tetrahydroquinolines in excellent yields. It is worth mentioning some of the 1,2,3,4-tetrahydroquinolines presented in Scheme 1 serve as precursors or intermediates for the synthesis of bioactive molecules. In particular, products **1**, **2** and **11** can result in 5-HT3 receptor antagonists, antitrypanosomally drugs and tubulin polymerization inhibitors.[14] Following the selective hydrogenation of quinolines, we became interested in the hydrogenation of other N-heterocycles. First, quinoxaline could be converted to the corresponding hydrogenated product (Scheme 2, product **16**) under very mild conditions. In addition, 2-methyl-1,2,3,4-tetrahydroquinoxaline (Scheme 2, product **17**) was obtained for the first time with a nanostructured cobalt catalyst in good yield under mild reaction conditions. Next, we were interested in the hydrogenation of pyridines and pyrroles to demonstrate the superior

general applicability of our cobalt catalyst. To achieve good yields, the reaction conditions had to be modified and required 5.0 MPa H_2, 120 °C and 10 mol% Co. Under these conditions, we were able to hydrogenate pure pyridine efficiently (Scheme 2, product **18**) as well as isonicotinamide (Scheme 2, product **19**) which is known as a reversible organic hydrogen storage liquid for potential hydrogen-powered fuel cells in mobile applications.[15] Simple pyrrole and 2-methylpyrrole (Scheme 2, products **20** and **21**) could be also converted to the corresponding hydrogenated products in good yields. We further tested our catalyst in the hydrogenation of indoles. 2-methylindole as well as 2,3,3-trimethylindolenin can be converted to the products in excellent yields (Scheme 2, product **22** and **23**). Indolines and their scaffold are known as important pharmaceuticals and agrochemicals and it is particularly useful to have a selective and simple access to this class of compounds.[16] As a consequence, hydrogenation catalysis has been used to synthesize indolines.[17] The reduction of isoquinoline (Scheme 2, product **24**) was also performed. It is noteworthy, that drastic conditions are needed for complete selective hydrogenation compared to quinoline. When our catalyst is used with 9-aminoacridine, we selectively obtain 1,2,3,4,5,6,7,8-octahydro-9-aminoacridine (Scheme 2, product **25**). This is in contrast to the other products, as we were able to selectively hydrogenate the phenyl rings instead of the N-heterocycle. We assume that partial hydrogenation takes place in the N-heterocycle part and subsequent rearrangement. In the case of phenanthroline and benzo*[h]*quinoline, we were also able to selectively reduce the N-heteroarene rings and the corresponding partially reduced products were obtained in up to 81% yield (Scheme 2, products

Chemistry–A European Journal

Research Article
doi.org/10.1002/chem.202300561

Chemistry Europe
European Chemical
Societies Publishing

Scheme 1. Hydrogenation of quinolines to the corresponding 1,2,3,4-tetrahyrodquinolines. Reaction conditions: 5.0 mol% Co (1.81 wt.% Co, 0.01 mmol Co, 0.59 mg Co), 0.2 mmol substrate, 3 mL ethanol, 70 °C, 2.0 MPa H_2, 20 h. Isolated yields are given.

Scheme 2. Products of the hydrogenation of different N-, O-, and S-heterocycles. Reaction conditions: 5.0 mol% Co (1.81 wt.% Co, 0.01 mmol Co, 0.59 mg Co), 0.2 mmol substrate, 3 mL ethanol, 70 °C, 2.0 MPa H_2, 20 h. Isolated yields are given. [a] 10 mol% Co (1.81 wt.% Co, 0.02 mmol Co, 1.18 mg Co), 0.2 mmol substrate, 3 mL ethanol, 120 °C, 5.0 MPa H_2, 20 h. Isolated yields are given. [b] 5 mol% Co (1.81 wt.% Co, 0.01 mmol Co, 0.59 mg Co), 0.2 mmol substrate, 3 mL ethanol, 100 °C, 3.0 MPa H_2, 20 h. Isolated yields are given. [c] 15 mol% Co (1.81 wt.% Co, 0.03 mmol Co, 1.77 mg Co), 0.2 mmol substrate, 3 mL ethanol, 150 °C, 6.0 MPa H_2, 48 h. Isolated yields are given.

26 and **27**). In addition to N-heterocycles, we applied our catalyst to the more challenging hydrogenation of O- and S-heterocycles. The selective hydrogenation of benzofurans is of great interest[9,18,19] because the associated products are important bio-active molecules. With our catalyst, we are able to selectively hydrogenate benzofuran to 2,3-dihydrobenzofuran (Scheme 2, product **28**). We had to modify the initial conditions slightly i.e. 3.0 MPa H_2 and 100 °C to obtain an excellent yield. Moreover, we could also demonstrate the selective hydrogenation of 5-bromobenzofuran (Scheme 2, product **29**). Having shown the successful hydrogenation of N- and O-heterocycles, the compounds 5-methylbenzothiophene and 4-chlorobenzothiophene were hydrogenated. To achieve a reasonable yield, we had to modify the reaction conditions by using 6.0 MPa H_2, 150 °C, 48 h and 15 mol% Co (Scheme 2, product **30** and **31**). The hydrogenation of benzothiophenes is very challenging and research has focused on benzothiophene.[19,20] The strong binding of sulfur containing heterocycles to the active metal sites is an additional hurdle.[21] Very recently and parallel to our work, Beller/Jagadeesh and coworkers introduced an earth abundant metal based heterogeneous catalyst system able to hydrogenate benzofuran derivatives and benzothiophenes.[22]

Regarding reusability, five consecutive runs were carried out (Supporting Information 4.3) and the yields and initial rates obtained indicate very good recyclability. As observed by TEM measurements, there is no agglomeration or growing of nanoparticles in the used catalyst during catalysis. Moreover, particle size distribution after catalysis with an average diameter of 6.2 nm has been observed (Supporting Information 4.4.1). In addition, a hot filtration test was performed, and the separated solution showed no activity. This indicates that irreversibly leached cobalt species play no significant role in arene hydrogenation catalysis. The leaching of our catalyst was determined by ICP-OES and found to be 0.7% (Supporting Information 4.4.3). To demonstrate the efficiency and practicality of our cobalt catalyst, an upscaling of the benchmark reaction was

Chemistry–A European Journal

Research Article
doi.org/10.1002/chem.202300561

Chemistry Europe
European Chemical
Societies Publishing

performed using 10 mmol quinoline. This resulted in the isolated yield of 90% of 1,2,3,4-tetrahydroquinoline (Supporting Information 4.5).

Conclusion

In conclusion, we introduced a protocol to synthesize highly active and selective nano-structured 3d-metal catalysts and succeeded in identifying a selective cobalt hydrogenation catalyst. A variation in the ratio of metal to N/C precursor can be used to boost catalyst performance. Our catalyst can operate under very mild conditions permitting the hydrogenation of numerous classes of N-, O- and S-heterocycles selectively. The discovered catalyst synthesis protocol might assist others to find selective and highly active nanostructured 3d-metal catalysts for arene hydrogenation and other important catalytic transformations.

Experimental Section

Catalyst synthesis: To a suspension of meso-octamethylcalix[4]pyrrole (1.352 mmol, 579.32 mg) in 12 mL MeOH, $Co(OAc)_2 \cdot 4 H_2O$ (0.338 mmol, 84.16 mg, 4 wt.% ideally) is added to 500 mg SiO_2 and the solvent is evaporated at 70°C under slow, constant stirring. The active catalyst material is generated by pyrolysis at 800°C under nitrogen flow, followed by pyrolysis at 550°C under nitrogen flow.

Catalyst characterization: TEM was carried out by using a JEOL JEM 2200FS (200 kV) device. For the sample preparation, the samples were suspended in chloroform and sonicated for 5 min. For analysis, LC200-Cu grids were used. Scanning transmission electron microscopy (STEM) measurements were performed using a JEM-ARM200F (JEOL) equipped with a cold emission gun, a STEM probe corrector (CEOS GmbH), and an energy filter (GATAN). The microscope was operated at 200 kV with a probe current of 80 pA. The probe convergence semi-angle was 13.4 mrad (20 μm condenser lens aperture). The images were recorded with an annular dark-field (ADF) detector using a detector distance of 8 cm resulting in a collection angle of 68–280 mrad. The image size, pixel size, and pixel dwell time of the STEM images were 1024×1024 pixels, 0.063 nm, and 16 μm, respectively. Electron energy loss spectroscopy (EELS) measurements were performed in STEM mode with the same probe size, condenser lens aperture, and detector distance. The energy dispersion of the spectrometer was set to 0.25 eV. The image collection semi-angle was 20.8 mrad. The image size, pixel size, and pixel dwell time of the EELS spectrum images were 100×100 pixels, 0.33 nm, and 20 ms, respectively. X-ray photoelectron spectroscopy (XPS) was performed using a Physical Electronics Phi 5000 Versa Probe III instrument. As X-ray source a monochromatic Al Kα with a spot size of 100 μm (21.1 W) was used. The kinetic pass energy of the photoelectrons was determined with a hemispheric analyzer (45°) set to pass energy of 13 eV for high-resolution spectra. Pore characterizations were carried out via nitrogen physisorption measurements using a Nova2000e (Quantochrome) apparatus. The pore size distribution was computed via DFT calculations (calculation model: N_2 at −196.15°C: slit/cylindrical pore, NLDFT equilibrium model). The specific surface area was calculated using p/p_0 values from 0.05–0.3 (BET). PXRD and PDF measurements have been taken at the European Synchrotron Radiation Facility (ESRF), beamline ID-15 A, which is equipped with a PILATUS 2 M, S/N 24-0131, X series detector. The powder was

packed in Lindemann special glass capillaries with a diameter of 1 mm. Measurements were made for one minute at a photon energy of 90 keV (30 images each 2 seconds). Distance calibration was done with a CeO_2, NIST 674b standard.

General procedure for the hydrogenation of aromatic heterocycles: A 10 mL glass reaction vial was charged with a magnetic stirring bar, 0.2 mmol substrate, 3 mL EtOH and 32.6 mg catalyst (5.0 mol% Co). The vial was placed in a 300 mL high-pressure autoclave (Parr Instruments). The autoclave was flushed three times with 2.0 MPa hydrogen. Afterwards, 2.0 MPa hydrogen was applied, and the reaction was stirred at 70°C for 20 h. After completion of the reaction time, the autoclave was cooled to room temperature and the hydrogen was released. The catalyst was removed by filtration. The solvent was removed via rotary evaporation and high vacuum. After purification via column chromatography, the product was analysed by ^1H- and ^{13}C NMR spectroscopy. NMR measurements were performed using a Varian INOVA 300 (300 MHz for ^1H, 75 MHz for ^{13}C) and a Varian INOVA 400 (400 MHz for ^1H, 100 MHz for ^{13}C) instrument at 296 K. For certain substrates, hydrogen pressure, temperature and reaction time as well as catalyst loading have been adapted.

Conflict of Interest

The authors declare no conflict of interest.

Data Availability Statement

The data that support the findings of this study are available in the supplementary material of this article.

[1] K. Weissermel, H.-J. Arpe, *Industrial Organic Chemistry*, Wiley-VCH, Weinheim, **2008**.

[2] P. G. Andersson, *Modern Reduction Methods*, John Wiley & Sons Incorporated, Weinheim, **2008**.

[3] a) M. S. Salman, N. Rambhujun, C. Pratthana, K. Srivastava, K.-F. Aguey-Zinsou, *Ind. Eng. Chem. Res.* **2022**, *61*, 6067–6105; b) Y. Jo, J. Oh, D. Kim, J. H. Park, J. H. Baik, Y.-W. Suh, *Korean J. Chem. Eng.* **2022**, *39*, 20–37; c) K. C. Tan, T. He, Y. S. Chua, P. Chen, *J. Phys. Chem. C* **2021**, *125*, 18553–18566.

[4] a) M. El-Shahat, *J. Heterocycl. Chem.* **2022**, *59*, 399–421; b) M. P. Wiesenfeldt, Z. Nairoukh, T. Dalton, F. Glorius, *Angew. Chem. Int. Ed.* **2019**, *58*, 10460–10476; *Angew. Chem.* **2019**, *131*, 10570–10586; c) Z.

Wei, F. Shao, J. Wang, *Chin. J. Catal.* **2019**, *40*, 980–1002; d) A. Gualandi, D. Savoia, *RSC Adv.* **2016**, *6*, 18419–18451.

[5] F. Chen, A.-E. Surkus, L. He, M.-M. Pohl, J. Radnik, C. Topf, K. Junge, M. Beller, *J. Am. Chem. Soc.* **2015**, *137*, 11718–11724.

[6] K. Murugesan, V. G. Chandrashekhar, C. Kreyenschulte, M. Beller, R. V. Jagadeesh, *Angew. Chem. Int. Ed.* **2020**, *132*, 17561–17565.

[7] W. Gong, Q. Yuan, C. Chen, Y. Lv, Y. Lin, C. Liang, G. Wang, H. Zhang, H. Zhao, *Adv. Mater.* **2019**, *31*, e1906051.

[8] a) N. Antil, A. Kumar, N. Akhtar, W. Begum, M. Chauhan, R. Newar, M. S. Rawat, K. Manna, *Inorg. Chem.* **2022**, *61*, 1031–1040; b) F. Tang, G. Zhang, L. Wang, J. Huang, Y.-N. Liu, *J. Catal.* **2022**, *414*, 101–108; c) V. M. Asaula, V. V. Buryanov, B. Y. Solod, D. M. Tryus, O. O. Pariiska, I. E. Kotenko, Y. M. Volovenko, D. M. Volochnyuk, S. V. Ryabukhin, S. V. Kolotilov, *Justus Liebigs Ann. Chem.* **2021**, *2021*, 6616–6625; d) M. Puche, L. Liu, P. Concepción, I. Sorribes, A. Corma, *ACS Catal.* **2021**, *11*, 8197–8210; e) R. Huang, C. Cao, J. Liu, L. Zheng, Q. Zhang, L. Gu, L. Jiang, W. Song, *ACS Appl. Mater. Interfaces.* **2020**, *12*, 17651–17658; f) J. Hervochon, V. Dorcet, K. Junge, M. Beller, C. Fischmeister, *Catal. Sci. Technol.* **2020**, *10*, 4820–4826; g) Z.-H. He, Y.-C. Sun, K. Wang, Z.-Y. Wang, P.-P. Guo, C.-S. Jiang, M.-Q. Yao, Z.-H. Li, Z.-T. Liu, *J. Mol. Catal.* **2020**, *496*, 111192; h) G. Jaiswal, M. Subaramanian, M. K. Sahoo, E. Balaraman, *ChemCatChem* **2019**, *11*, 2449–2457; i) I. Sorribes, L. Liu, A. Doménech-Carbó, A. Corma, *ACS Catal.* **2018**, *8*, 4545–4557; j) J. Li, G. Liu, X. Long, G. Gao, J. Wu, F. Li, *J. Catal.* **2017**, *355*, 53–62; k) Z. Wei, Y. Chen, J. Wang, D. Su, M. Tang, S. Mao, Y. Wang, *ACS Catal.* **2016**, *6*, 5816–5822; l) J. E. Shaw, P. R. Stapp, *J. Heterocycl. Chem.* **1987**, *24*, 1477–1483.

[9] P. Ji, K. Manna, Z. Lin, A. Urban, F. X. Greene, G. Lan, W. Lin, *J. Am. Chem. Soc.* **2016**, *138*, 12234–12242.

[10] a) C. Bäumler, C. Bauer, R. Kempe, *ChemSusChem* **2020**, *13*, 3110–3114; b) G. Hahn, P. Kunnas, N. de Jonge, R. Kempe, *Nat. Catal.* **2019**, *2*, 71–77; c) T. Schwob, P. Kunnas, N. de Jonge, C. Papp, H.-P. Steinrück, R. Kempe, *Sci. Adv.* **2019**, *5*, eaav3680.

[11] J. A. Shriver, S. G. Westphal, *J. Chem. Educ.* **2006**, *83*, 1330–1332.

[12] A. Khort, S. Roslyakov, P. Loginov, *Nano-Struct. Nano-Objects* **2021**, *26*, 100727.

[13] F. H. Allen, O. Kennard, D. G. Watson, L. Brammer, A. G. Orpen, R. Taylor, *J. Chem. Soc. Perkin Trans. 1* **1987**, S1.

[14] a) V. Sridharan, P. A. Suryavanshi, J. C. Menéndez, *Chem. Rev.* **2011**, *111*, 7157–7259; b) R. J. Pagliero, S. Lusvarghi, A. B. Pierini, R. Brun, M. R. Mazzieri, *Bioorg. Med. Chem.* **2010**, *18*, 142–150; c) J.-P. Liou, Z.-Y. Wu, C.-C. Kuo, C.-Y. Chang, P.-Y. Lu, C.-M. Chen, H.-P. Hsieh, J.-Y. Chang, *J. Med. Chem.* **2008**, *51*, 4351–4355.

[15] Y. Cui, S. Kwok, A. Bucholtz, B. Davis, R. A. Whitney, P. G. Jessop, *New J. Chem.* **2008**, *32*, 1027–1037.

[16] a) I. V. Ukrainets, N. L. Bereznyakova, *Chem. Heterocycl. Compd.* **2012**, *48*, 155–165; b) Y.-J. Wu in *Topics in Heterocyclic Chemistry, Vol. 26* (Ed.: G. W. Gribble), Springer, Heidelberg, **2010**, pp. 1–29; c) E. Lacivita, M. Leopoldo, *Curr. Top. Med. Chem.* **2006**, *6*, 1927–1970.

[17] a) S. Zhang, J. Gan, Z. Xia, X. Chen, Y. Zou, X. Duan, Y. Qu, *Chem* **2020**, *6*, 2994–3006; b) H. Bernas, N. Kumar, A. Aho, R. Leino, D. Y. Murzin, *Catal. Commun.* **2014**, *56*, 41–44; c) H. Cho, F. Török, B. Török, *Org. Biomol. Chem.* **2013**, *11*, 1209–1215; d) D. Clarisse, B. Fenet, F. Fache, *Org. Biomol. Chem.* **2012**, *10*, 6587–6594; e) A. Kulkarni, W. Zhou, B. Török, *Org. Lett.* **2011**, *13*, 5124–5127.

[18] a) A. Hamza, D. Moock, C. Schlepphorst, J. Schneidewind, W. Baumann, F. Glorius, *Chem. Sci.* **2022**, *13*, 985–995; b) D. Timelthaler, C. Topf, *Synthesis* **2022**, *54*, 629–642; c) D. Moock, T. Wagener, T. Hu, T. Gallagher, F. Glorius, *Angew. Chem. Int. Ed.* **2021**, *60*, 13677–13681; *Angew. Chem.* **2021**, *133*, 13791–13796; d) S. Rengshausen, C. van Stappen, N. Levin, S. Tricard, K. L. Luska, S. DeBeer, B. Chaudret, A. Bordet, W. Leitner, *Small* **2021**, *17*, e2006683; e) Y. Ge, Z. Wang, Z. Han, K. Ding, *Chem. Eur. J.* **2020**, *26*, 15482–15486; f) S. El Sayed, A. Bordet, C. Weidenthaler, W. Hetaba, K. L. Luska, W. Leitner, *ACS Catal.* **2020**, *10*, 2124–2130; g) X. Long, Z. Li, G. Gao, P. Sun, J. Wang, B. Zhang, J. Zhong, Z. Jiang, F. Li, *Nat. Commun.* **2020**, *11*, 4074; h) K. Murugesan, T. Senthamarai, A. S. Alshammari, R. M. Altamimi, C. Kreyenschulte, M.-M. Pohl, H. Lund, R. V. Jagadeesh, M. Beller, *ACS Catal.* **2019**, *9*, 8581–8591; i) P. Ji, P. Song, T. Drake, S. S. Veroneau, Z. Lin, X. Pan, W. Lin, *J. Am. Chem. Soc.* **2018**, *140*, 433–440; j) A. Karakulina, A. Gopakumar, Z. Fei, P. J. Dyson, *Catal. Sci. Technol.* **2018**, *8*, 5091–5097; k) H. Jiang, J. Xu, B. Sun, *Appl. Organomet. Chem.* **2018**, *32*, e4260; l) T.-N. Ye, J. Li, M. Kitano, H. Hosono, *Green Chem.* **2017**, *19*, 749–756; m) A. Karakulina, A. Gopakumar, İ. Akçok, B. L. Roulier, T. LaGrange, S. A. Katsyuba, S. Das, P. J. Dyson, *Angew. Chem. Int. Ed.* **2016**, *128*, 300–304; n) L. Pauli, R. Tannert, R. Scheil, A. Pfaltz, *Chem. Eur. J.* **2015**, *21*, 1482–1487; o) Y. Gong, P. Zhang, X. Xu, Y. Li, H. Li, Y. Wang, *J. Catal.* **2013**, *297*, 272–280; p) C. Liu, Z. Rong, Z. Sun, Y. Wang, W. Du, Y. Wang, L. Lu, *RSC Adv.* **2013**, *3*, 23984–23988; q) N. Ortega, S. Urban, B. Beiring, F. Glorius, *Angew. Chem. Int. Ed.* **2012**, *51*, 1710–1713; *Angew. Chem.* **2012**, *124*, 1742–1745; r) N. Ortega, B. Beiring, S. Urban, F. Glorius, *Tetrahedron* **2012**, *68*, 5185–5192; s) M. Maris, W.-R. Huck, T. Mallat, A. Baiker, *J. Catal.* **2003**, *219*, 52–58.

[19] H. Jiang, S. Zhang, B. Sun, *Catal. Lett.* **2018**, *148*, 1336–1344.

[20] a) M. Fang, R. A. Sánchez-Delgado, *J. Catal.* **2014**, *311*, 357–368; b) K. Okamoto, R. Akiyama, S. Kobayashi, *J. Org. Chem.* **2004**, *69*, 2871–2873.

[21] J. Oudar, *Catal. Rev.* **1980**, *22*, 171–195.

[22] B. Zhou, V. G. Chandrashekhar, Z. Ma, C. Kreyenschulte, S. Bartling, H. Lund, M. Beller, R. V. Jagadeesh, *Angew. Chem. Int. Ed.* **2023**, e202215699.